Hybrid SAR Speckle Reduction Using Complex Wavelet Shrinkage and Non-Local PCA-Based Filtering

Ramin Farhadiani, Saeid Homayouni, *Senior Member, IEEE*, and Abdolreza Safari,

In this paper, a new hybrid despeckling method, based on Undecimated Dual-Tree Complex Wavelet Transform (UDT-CWT) using *maximum a posteriori* (MAP) estimator and non-local Principal Component Analysis (PCA)-based filtering with local pixel grouping (LPG-PCA), was proposed. To achieve a heterogeneous-adaptive speckle reduction, SAR image is classified into three classes of point targets, details, or homogeneous areas. The despeckling is done for each pixel based on its class of information. Logarithm transform was applied to the SAR image to convert the multiplicative speckle into additive noise. Our proposed method contains two principal steps. In the first step, denoising was done in the complex wavelet domain via MAP estimator. After performing UDT-CWT, the noise-free complex wavelet coefficients of the log-transformed SAR image were modeled as a two-state Gaussian mixture model. Furthermore, the additive noise in the complex wavelet domain was considered as a zero-mean Gaussian distribution. In the second step, after applying inverse UDT-CWT, an iterative LPG-PCA method was used to smooth the homogeneous areas and enhance the details. The proposed method was compared with some state-of the-art despeckling methods. The experimental results showed that the proposed method leads to a better speckle reduction in homogeneous areas while preserving details.

Index Terms—**Gaussian mixture model, homomorphic transformation, non-local filtering, undecimated dual-tree complex wavelet transform.**

I. INTRODUCTION

Synthetic Aperture Radar (SAR) images are inherently affected by a signal-dependent granular noise-like phenomenon called speckle, which is the nature of all coherent systems. The presence of speckle in the SAR images decreases the performance of various pattern recognition applications such as classification, change detection, and biomass estimation. Hence, a primary preprocessing step, namely despeckling, is needed to suppress the speckle phenomena.

As yet, various spatial domain filters have been proposed in the literature for reducing the speckle in SAR images; among others, Lee [1], Frost [2], and Kuan [3] are the most popular and frequently used filters. Although these methods have a decent ability to smooth flat areas, they suffer from many problems.

For example, they are sensitive to the size and shape of the used kernel.

Multi-Resolution Analysis (MRA) method, introduced in the early 1990s, can overcome the before mentioned disadvantages of spatial filters. Wavelet transform, with all its variation and further developments, has been extensively used for denoising images that corrupted with Additive White Gaussian Noise (AWGN) and speckle. However, speckle in SAR images has multiplicative nature and should be converted to an additive one. For this propose, the first solution is using the logarithm transform (homomorphic filtering) and the second one is conducted by rewriting the observed signal as a sum of signal and signal dependent noise (non-homomorphic filtering) [4]–[6]. However, denoising in the wavelet domain can be done by thresholding the wavelet coefficients or by employing the Bayesian theory. The performance of speckle reduction methods based on Bayesian theory is highly dependent on the appropriate probability distribution function (PDF) that was used as a prior model for describing the noise-free wavelet coefficients. In [7], Mallat described that the distribution of wavelet coefficients is non-Gaussian, symmetric, and sharply peaked around zero with heavy tails. To capture this heavy-tailed property, various PDFs, e.g., Cauchy [8], [9], bivariate Cauchy [10], Gaussian mixture [11], [12], and Laplace mixture [13], [14] PDFs within the MAP, MMSE, and MMAE estimators in the Wavelet, Dual-Tree Complex Wavelet, Contourlet, Directionlet, and Lapped Domains have been used in the literature. However, these methods may have some limitations, such as presented ringing effect near edges or isolated patterns in homogeneous areas, which make the despeckling results visually annoying.

Recently, with the advent of non-local means filtering (NLM) [15] for reducing the additive Gaussian noise, this idea was extended to suppress the speckle from SAR images [16]–[25], as well as Polarimetric SAR image despeckling [26], [27]. Besides these non-local despeckling approaches, some despeckling methods based on neural networks [28]–[30] and total variation [31], [32] were also presented in the literature.

As mentioned in [33], a suitable SAR speckle reduction method must satisfy the following characteristics: 1) reduce speckle in homogeneous areas; 2) preserve details of SAR image such as edges, texture, point targets, and urban areas; 3) radiometric preservation; and 4) artifact-free. In this article, we proposed a novel hybrid heterogeneous-adaptive speckle reduction method based on complex wavelet shrinkage and non-local Principal Component Analysis (PCA)-based filtering. Since the classic wavelet transform has some limitations and suffers from several fundamental shortcomings such as the lack of shift invariance and poor directional selectivity [34], we utilized the Undecimated Dual-Tree Complex Wavelet Transform (UDT-CWT) [35] that is shift invariant and isolate edges with different orientations in different subbands. Also, we used non-local PCA-based denoising with local pixel grouping (LPG-PCA) [36] in our proposed method. First, by some predefined kernels, three classes of heterogeneity, e.g., point targets, details (contain lines and edges), or homogeneous areas are extracted from the SAR image. After that, our proposed method starts with two principal steps. In the first step, despeckling was done in the complex wavelet domain within *maximum a posteriori* (MAP) estimator. In the second step, by employing an iterative LPG-PCA method, the flat areas were completely smoothed, and the details were enhanced.

II. Proposed Despeckling Method

If S is theoretically noise-free SAR image (or reflectivity) and η is fully developed speckle, then the model of observed SAR image I can be expressed as $I = S \cdot \eta$ [33]. From this equation, we can find that speckle is multiplicative phenomenon in nature. To convert this multiplicative noise into an additive one, we can take a logarithm transform from both sides of this equation and we have

$$Z = X + N \qquad (1)$$

where Z, X, and N are the logarithm transform of I, S and η, respectively. In the next subsections, we describe how to classify the SAR image into various classes of heterogeneity, and explain how to use these classes to better suppress the speckle from a SAR image.

A. *Classification Strategy*

To achieve a heterogeneous-adaptive speckle reduction, many methods have been proposed in the literature [4]–[6], [12], [14], [20], [23]. In this article, we used the ratio detector to classify SAR image. In this method, each pixel was classified into three classes of heterogeneity such as point targets, details, or homogeneous areas. To this end, we proposed to use common ratio detectors [37]. The kernels that are used to identify the point targets, lines, and edges are shown in Fig. 1. To decrease the computational cost, we used predefined fixed-size 11×11 kernels. The ratio detector to point targets detection can be computed as $R_{pt} = R_2 / R_1$ where R_1 and R_2 represent the average of values in dark and white pixels in the defined kernel, respectively. If R_{pt} is smaller (or equal) than the threshold T_{pt}, the pixel will be assigned as point target. In the case of edges and lines detection, the ratio detector can be defined as

$$R_{e-l} = \begin{cases} R_1/R_2 & if \quad R_1/R_2 \le 1 \\ R_2/R_1 & if \quad R_2/R_1 \le 1 \end{cases} \qquad (2)$$

After computing R_{e-l} for each direction, the minimum value of R_{e-l} will be considered as the direction of the interested pixel. It should be noted that the different kernels were used to identify the lines (Fig. 1b) and the edges (Fig. 1c). After that, the edges and lines maps will be fused together to achieve fusion map as

$$\mathrm{map}_f = \sqrt{(\mathrm{map}_e^2 + \mathrm{map}_l^2)}/2 \qquad (3)$$

where map_e, map_l, and map_f represent the edges, lines, and fused maps, respectively. In the last stage, the map_f has to be normalized between [0, 1]. The final details map can be computed as $\mathrm{map}_f < T_d$, where T_d is a threshold. It should be noted that choosing a small T_{pt} or T_d can cause fewer point targets and details detection, respectively. While larger thresholds can find more pixels as point targets and details. For this reason, T_{pt} and T_d should be chosen based on the content of the SAR image. To achieve better classification result, we performed a light low-pass Gaussian filter on the SAR image before applying the classification strategy. Also, to remove the false detected details, especially in the case of single-look SAR image, by employing a local 3×3 window, we will remove the neighbors that contain details fewer than 4 pixels. Fig. 2 shows a single-look real SAR data named Toronto. Moreover, this figure represents point targets and details maps. After classifying the SAR image into three classes, the speckle suppression is done based on each class information. To save the point targets, they will be completely excluded from the despeckling process and, at the end, they will be back to their original locations.

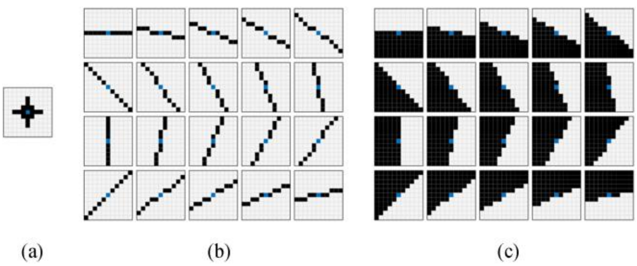

Fig. 1. Kernels for pixel classification. (a) Point target. (b) Line. (c) Edge.

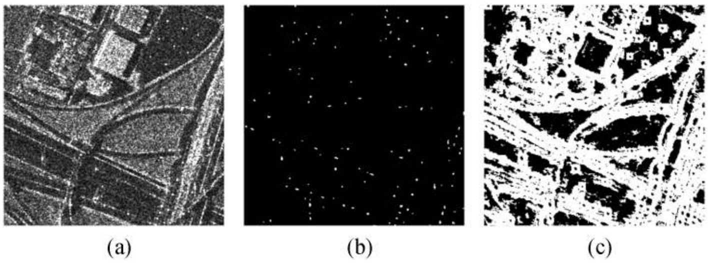

Fig. 2. Classification result. (a) Real SAR image. (b) Point targets map. (c) Final details map.

B. *Step 1*

In this step, the homogeneous areas were despeckled in the complex wavelet domain, and also a light despeckling was performed on the detected details. In (1), we assume that the signal and noise components are independent random variables and N is considered as an additive noise. Because the UDT-CWT is a linear transformation, after applying it to (1) to up to scale j, the noisy complex wavelet coefficients y at each scale can be written as $y_j^i = w_j^i + n_j^i$ where w and n are the noise-free coefficients and the noise component, respectively. Also, subscript i denotes the orientations $\pm 15^{\circ}, \pm 45^{\circ}, \pm 75^{\circ}$. For the sake of clarity, we omitted j and i. Our goal here is to estimate w from the noisy observation y. For this purpose, we used the MAP estimator. The Bayesian MAP estimator can be written as

$$\hat{w}(y) = \arg\max_{\hat{w}} [p_n(y-n) p_w(w)] \qquad (4)$$

where $p_n(y-n)$ and $p_w(w)$ are the noise component and the noise-free complex wavelet coefficients, respectively. In the proposed method, the noise component in the complex wavelet domain assumed to be zero mean Gaussian PDF with the standard deviation σ_n. By considering this assumption, if $p_w(w)$ is assumed to be a zero-mean Gaussian density with standard deviation σ_n, then the estimator can be written as $\hat{w}(y) = (\sigma^2/\sigma^2 + \sigma_n^2).y$ [38]. In this equation, σ_n is unknown and it can be estimated by a robust median estimator from subband HH in the first and second scales of the complex wavelet coefficients as $\hat{\sigma}_n = (D_1 + D_2)/2$ [39], where D_i can be computed as $D_i = \text{median}(|HH_i|)/0.6745, i = 1, 2$ [40]. As mentioned before, a proper speckle reduction filtering has to flat the homogeneous areas while preserving the image features and their corresponding spatial information. To this end, an additional parameter, namely smoothing factor (C), is multiplied into $\hat{\sigma}_n$. Here, we introduce two types of C factors: C_h for homogeneous class and C_d for details class. These two parameters have to be tuned according to the content of the image. In low signal-to-noise ratio images, e.g., single-look SAR image, C_h might have a large value. However, if C_h is too large, the image will be over-smoothed. In contrast, by increasing the number of looks, speckle in the SAR image decreases. Hence, we can choose a lower value for C_h. Based on our experiments, for the homogeneous class, the C_h is in the range between one and three. However, for details class, C_d must be chosen below one, in order to preserve the details and perform light noise reduction on them.

In this paper, we will employ a two-state Gaussian mixture PDF for modeling $p_w(w)$ as

$$p_w(w) = \alpha_1 p_1(w) + \alpha_2 p_2(w) = \alpha_1 . \frac{1}{\sigma_1^2\sqrt{2}} \exp\left(-\frac{w^2}{2\sigma_1^2}\right) + \alpha_2 . \frac{1}{\sigma_2^2\sqrt{2}} \exp\left(-\frac{w^2}{2\sigma_2^2}\right) \qquad (5)$$

where σ_1 and σ_2 denote the standard deviation of Gaussian components 1 and 2, respectively, whereas α_1 and α_2 represent their corresponding weights. In (5), σ_1, σ_2, α_1 and α_2 are unknown and should be estimated. For this purpose, we will use the iterative local Expectation-Maximization algorithm as descried in [12]. Computing the unknown parameters locally can increase the performance of the despeckling. If the window size is too big, the estimated parameters were closed to their global value. Based on our experimental results, we used a fixed-size 15×15 neighborhood for computing the parameters of the Gaussian mixture PDF. Because we use mixture PDF, we must use the averaged version of the MAP estimator (AMAP) [41] to estimate $\hat{w}$ from y. The AMAP estimator can be expressed as

$$\hat{w}(y) = \frac{\sum_{i=1}^{2} \alpha_i p_i \hat{w}_i}{\sum_{i=1}^{2} \alpha_i p_i} \qquad (6)$$

In the case of Gaussian noise, $\hat{w}$ is equal to $\hat{w}_i = (\sigma_i^2/\sigma_i^2 + \sigma_n^2).y, i = 1,2$. Because y is the sum of w and independent Gaussian noise, the PDF of y is the convolution of two independent Gaussian PDFs with variance σ_i^2 and σ_n^2, respectively. Therefore, p_i is a Gaussian PDF with variance $\sigma_i^2 + \sigma_n^2$ as $1/\sqrt{2\pi(\sigma_i^2 + \sigma_n^2)} \exp(-y^2/2(\sigma_i^2 + \sigma_n^2))$. Substituting $\hat{w}_i$ and p_i into (6) yields the following estimator:

$$\hat{w}(y) = \frac{\left(\sum_{i=1}^{2} \alpha_i \exp\left(-y^2/2(\sigma_n^2+\sigma_i^2)\right)\sigma_i^2\right)/\sqrt{2\pi(\sigma_n^2+\sigma_i^2)^3}}{\left(\sum_{i=1}^{2} \alpha_i \exp\left(-y^2/2(\sigma_n^2+\sigma_i^2)\right)\right)/\sqrt{2\pi(\sigma_n^2+\sigma_i^2)}} . y \qquad (7)$$

After denoising the all complex wavelet coefficients based on (7), the inverse UDT-CWT is applied.

C. *Step 2*

After despeckling the SAR image in the complex wavelet domain, we proposed to use the LPG-PCA method developed in [36]. Using the LPG-PCA method can efficiently decrease the undesired artifact that may appear in the homogeneous areas, as well as enhance the details. In this subsection, we will briefly describe the LPG-PCA method. For more details, we refer the readers to [36]. Since the remaining noise after taking inverse UDT-CWT is still additive in the log-transformed domain, by considering (1), the noise N and the noise-free data X assumed uncorrelated. Hence, the covariance matrix of Z can be calculated as $\Sigma_Z = \Sigma_X + \Sigma_N$, where Σ_N is equivalent to the noise variance (σ^2). The variance of the log-transformed speckle can be computed as $\psi(1, L)$ and $0.25 \times \psi(1, L)$ in the intensity and square root intensity SAR images, respectively, where L represents the number of looks and $\psi(1, L)$ denotes the first-order Polygamma function of L [42]. In this article, L is computed using an unsupervised method proposed in [43]. Like the smoothing factor defined in previous subsection, for reaching the better denoising result, we will multiply σ^2 into a positive constant θ. Similar to the smoothing factor, θ can control the level of noise reduction in the second step of the proposed algorithm. A large θ causes over-smoothing, while a small θ may not be able to reduce the noise in the SAR image. Based on our experiments, this parameter could be chosen above 1. In the LPG-PCA method, for a given pixel to be denoised, we considered an $M \times M$ variable block centered on it in which contains all the components within the window, and denoted by $= [z_1, \ldots, z_m]^T$, $m = M2$. In a variable block, we have $z = x + n$, where $x = [x_1, \ldots, x_m]^T$, $n = [n_1, \ldots, n_m]^T$. To calculating the PCA in order to estimate the x, we considered an $S \times S(S > M)$ training block around desired pixel. Here, we used a 41×41 training block, as well as a 7×7 variable block. In this method, selecting and grouping the training samples that are similar to the central $M \times M$ block is done based on block matching method. The matrix that contains the grouped patches can be written as $Z = [z^1, z^2, \ldots, z^n]$, where $z^k, k = 1, \ldots, n$ and $n = (S - M + 1)^2$ is the kth column vector of Z. In the next step, we should centralize the Z (e.g., $\bar{Z}$) as $\bar{z}^k = z^k - E(z^k)$, where $E(.)$ represents the expectation operation. After that, the PCA transform is applied on $\bar{Z}$ and we have $\Sigma_{\bar{Z}} = P \Lambda_{\bar{Z}} P^T$, where $\Sigma_{\bar{Z}}$, P, and $\Lambda_{\bar{Z}}$ denote the covariance matrix of the $\bar{Z}$, eigenvector, and diagonal eigenvalue matrixes, respectively. By applying P to the $\bar{Z}$, we have $\bar{Y}_N = P^T \bar{Z}$. Now, the Linear Minimum Mean Square Error (LMMSE) criterion is employed to reduce the noise component in $\bar{Y}_N$ and obtain $\hat{\bar{Y}}$ matrix. Finally, by reverse PCA transform and adding the mean values back, $\hat{X}$ is obtained.

Actually, most of the noise were removed in step 1 and step 2. However, we can iterate step 2 one more time to achieve a better denoising result. It should be noted that in the next iteration, σ^2 must be updated as

$$\sigma^2_{iter+1} = \left|\sigma^2_{iter} - E\left[\left(\hat{X}_{iter} - \hat{X}_{iter-1}\right)^2\right]\right|$$

where σ^2_{iter+1} is the variance of log-transformed speckle in the next iteration, $\hat{X}_{iter-1}$ is the estimated log-transformed SAR image in the previous iteration, and $E[.]$ denotes the expectation. It should be noticed here that to prevent the over-smoothing, we multiplied θ into σ^2 only in the first iteration. A block diagram of our proposed despeckling algorithm is also shown in Fig. 3. It should be noted that due to the use of the logarithmic transformation, the mean of the log-transformed speckle field is biased [44] and it is not equal to zero. Therefore, this biased mean should be corrected by subtracting the mean value of the log-transformed speckle from the output image of "step 2."

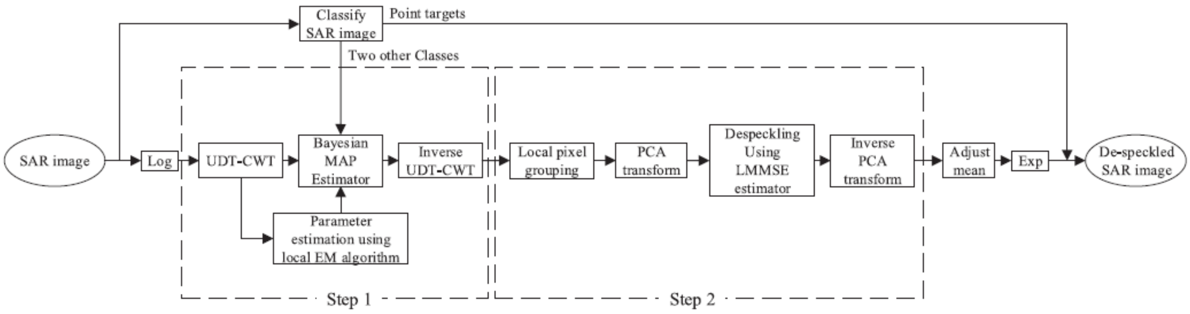

Fig. 3. The workflow of the proposed despeckling method.

III. EXPERIMENTAL RESULTS

This section presents the results of the performance analysis of the proposed speckle reduction method based on benchmarking data developed in [45] and two real SAR images (TerraSAR-X from Toronto, and AIRSAR over San Francisco). For comparison, we used several state-of-the-art despeckling methods. The first one is the iterative Probabilistic Patch-Based (PPB) [16] despeckling method. The iterative PPB method uses $\alpha = 0.92$, $T = 0.2$, 21×21 search window with a patch size of 7×7 and 25 iterations. Moreover, the SARBM3D [17] and FANS [18] despeckling methods were employed. The source codes of the PPB, SARBM3D, and FANS methods are available at [46], [47], and [48], respectively. For the proposed algorithm, four levels of complex wavelet decomposition were considered. Also, T_{pt} and T_d were equal to 0.25 and 0.65, for benchmarking datasets, as well as 0.5 and 0.78 for Toronto image and 0.5 and 0.85 for San Francisco image, respectively. Furthermore, C_h, C_d, and θ are considered as 0.3, 1, and 1.5 for benchmarking datasets; in addition, these parameters are equal to 0.1, 3, and 1.8 for Toronto image, as well as 0.1, 1, and 1.3 for San Francisco image, respectively.

A. *Performance Evaluation Using Benchmarking Data*

The benchmarking datasets used in this subsection were available at [49]. In this article, we only used some objective indicators proposed in [45] for single-look simulated Homogeneous, Digital Elevation Model (DEM), Squares, Corner, and Building reference datasets and we do not discuss how these datasets were generated or how to compute these indicators. For this reason, we refer the readers to [45] for more information. The refined version of Equivalent Number of Looks, referred as ENL*, was considered for Homogeneous image to evaluate the speckle suppression in homogeneous areas. The coefficient of variation (C_x) and Despeckling Gain (DG) were used for measuring the texture preservation and SNR improvement for DEM image. Figure of Merit (FOM) is employed as edge-preserving measuring indicator for Squares image. The contrast values C_{NN} and C_{BG} are used for evaluating the radiometric preservation through the filtering process in Corner image. C_{DR} and Building Smearing (BS), which respectively measure the radiometric precision and distortion of radiometric building profile in the range direction, were used for Building image. In the ideal case, the computed values for ENL*, DG, and FOM should be a large value; also, computed values for C_x , C_{NN} , C_{BG}, C_{DR}, and BS should be close to their clean values. As pointed out in [45], the goal of using these measuring datasets is not to find which method is better than others or which is the best one; nevertheless, it is to gain an insight about the ability and limitations of despeckling methods. Table I demonstrates the computed indicators for the PPB, SARBM3D, FANS, and the proposed method. All the results reported in Table I were obtained by averaging the despeckling results over eight independent single-look images of the same scene. Also, Fig. 4 represents clean, noisy, and despeckled images of each dataset. In Homogeneous image, our proposed method showed its ability to smooth flat areas. By the visual inspection, we can find that all methods generated some artifacts, especially in the SARBM3D and FANS outputs. In the DEM image, SARBM3D gained the nearest value to clean C_x ; also the best value for DG indicator was obtained by SARBM3D over 5 dB, followed by the FANS method. In the case of edge preserving, the PPB and SARBM3D methods have similar results and were the best. However, appearance of artifacts in flat areas is not deniable in all methods, especially in theSARBM3D and FANS results. In the case of corner reflector, the best strategy is to avoid perform any filtering on the detected corner reflector. By investigating the C_{NN} and C_{BG} values, we can find that our proposed method follows this strategy, as shown in Fig 4. Also, the SARBM3D and FANS methods provide acceptable results, except the PPB method which has lower C_{NN} and C_{BG} values. At the end, by investigating the C_{DR} and BS values, we can find that our proposed method has good performance to preserved building features.

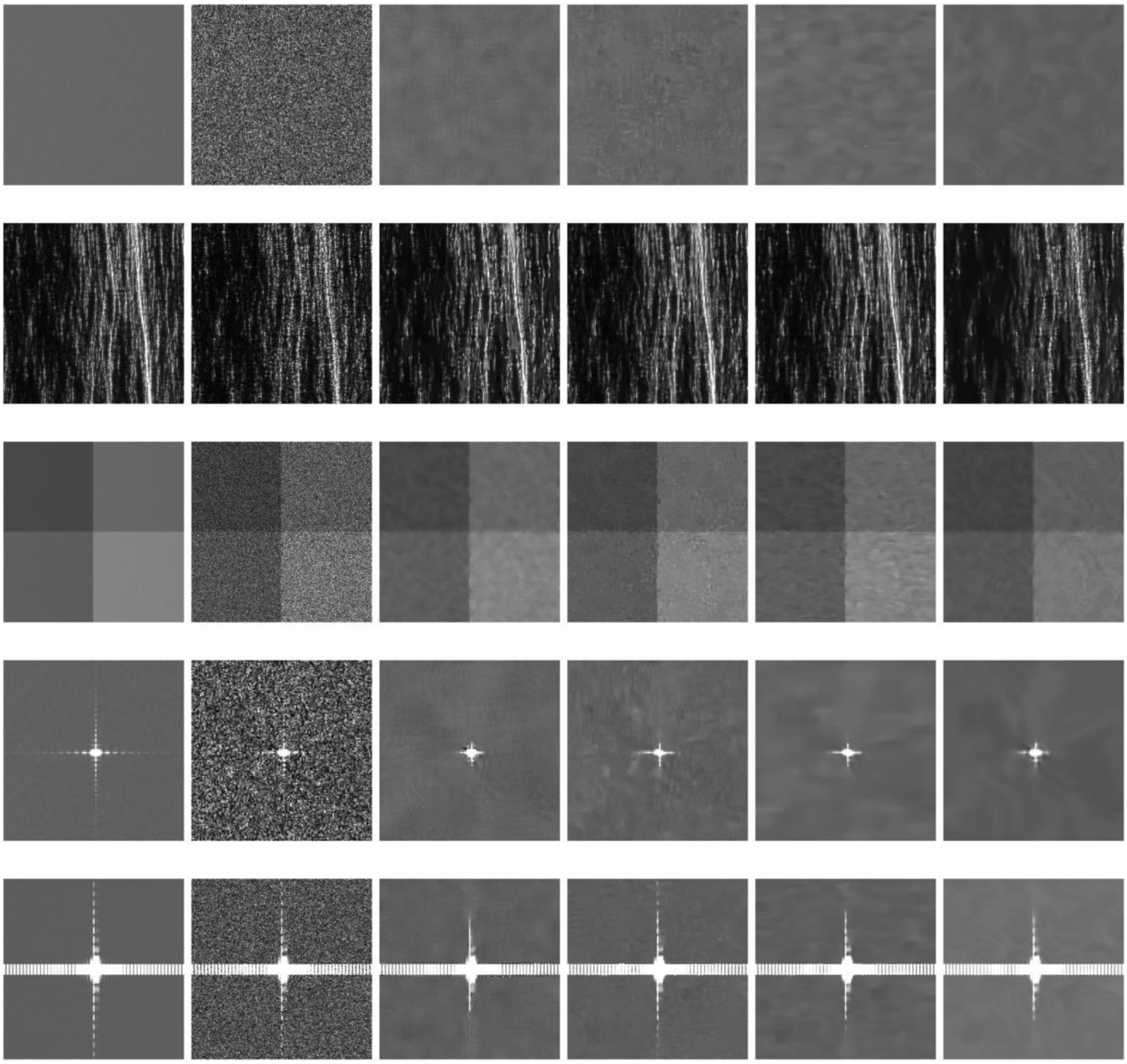

Fig. 4. From top to bottom, Homogeneous, DEM (256 × 256 zoomed area), Squares, Corner (128 × 128 zoomed area), and Building images, respectively. From left to right, clean, noisy, PPB, SARBM3D, FANS, and proposed method despeckling results, respectively.

TABLE I
PERFORMANCE COMPARISON ON THE BENCHMARKING DATASETS

		Clean	PPB	SARBM3D	FANS	Proposed
Hom.	ENL*	510.36	141.01	111.91	161.15	339.90
DEM	*Cx*	2.40	2.71	2.43	2.55	2.85
	DG	Inf	3.68	5.32	4.99	3.64
Squ.	FOM	0.926	0.819	0.818	0.799	0.797
Cor.	*CNN*	7.75	3.71	7.39	7.05	7.75
	CBG	36.56	32.70	35.45	35.37	37.14
Build.	*CDR*	65.90	64.90	65.91	65.66	64.44
	BS	0.00	3.13	1.46	3.51	0.58

B. *Performance Evaluation Using Real SAR Data*

The two real SAR images used in this subsection for performance evaluation are TerraSAR-X image of Toronto, Canada, 1-meter resolution, and AIRSAR L-band from San Francisco, USA, 10-meter resolution. These SAR datasets are in amplitude format for HH and VV polarization, respectively. The number of looks (L) of these datasets is considered to be about one and four for Toronto and San Francisco images, respectively. These datasets are presented in Fig. 5. To make a quantitative comparison, some numerical non-referenced indexes were used in this subsection, including Equivalent Number of Looks (ENL), Edge-Preservation Degree based on Ratio of Average (EPDROA), and Mean of Ratio image (MoR). The ENL is widely used to evaluate the speckle suppression in homogeneous areas. For the SAR image in amplitude format, the ENL can be computed as $(4/\pi - 1) \times (\mu/\sigma)^2$ [44], where μ and σ are mean and standard deviation values computed from a homogeneous area. The higher value of ENL represents the much speckle suppression. The EPD-ROA indicator can be computed as [50]

$$EPD - ROA = \frac{\sum_{i=1}^{N} |I_{S1}(i)/I_{S2}(i)|}{\sum_{i=1}^{N} |I_{I1}(i)/I_{I2}(i)|}$$

where I_{S1} and I_{S2} represent the adjacent pixel values of the despeckled image along horizontal or vertical direction, whereas I_{I1} and I_{I2} denote the corresponding adjacent pixel values of speckled image, respectively. In the ideal case, the EPD-ROA index is close to one and its value closer to one shows better edge preservation ability. The MoR between the SAR image before and after despeckling indicates the capability of the despeckling method for radiometric preservation, and in the ideal case, it should be equal to one. The results of despeckling of these two datasets are shown in Fig. 5. Also, Table II shows the computed values for various despeckling methods, regarding ENL and EPD-ROA in both horizontal and vertical directions and MoR. Among all despeckling methods, our proposed method achieves the better results, in terms of speckle reduction in homogeneous areas, while preserving the point targets and details. Also, Fig. 6 represents the zoomed area of Toronto image. By visual comparison of these figures, we can find that the SARBM3D method can preserve the details at the expense of poor speckle reduction in flat areas. The performance of the FANS method is better than the SARBM3D method, but it is still not the best. As the PPB method has effective speckle suppression and details preserving, it smoothed out some point targets, due to using a non-local approach, as can be seen from Fig. 6. Based on this figure, we observe that the proposed method has the best point targets preserving, while at the same time, the homogeneous areas are smooth and details are preserved. Also, with the analysis of MoR values, we can say that our proposed method has good ability to avoid radiometric distortion. As a result, we can say that our proposed method has a worthy performance in speckle suppression in homogeneous areas, while it preserves the point targets and details.

To evaluate the computational complexity of the despeckling methods, all the despeckling codes were executed on a PC with Intel Core i3-3220 CPU, 3.30 GHz, and 8 GB RAM. Also, the Toronto image (320 × 320) is employed for execution time comparison. The execution time of the methods was approximately around 108, 35, 4, and 92 s for the PPB, SARBM3D, FANS, and the proposed method, respectively. The FANS method have the fastest execution time, due to using variable-size search area, as well as probabilistic early termination approach and employing look-up tables. Although the PPB and the proposed method use non-local approach, their execution time is acceptable. However, the SARBM3D method is faster than the PPB and the proposed method. It should be noted that the proposed algorithm can achieve a better tradeoff between speckle reduction in homogeneous areas while preserving details and performing no-filtering on the point targets among others.

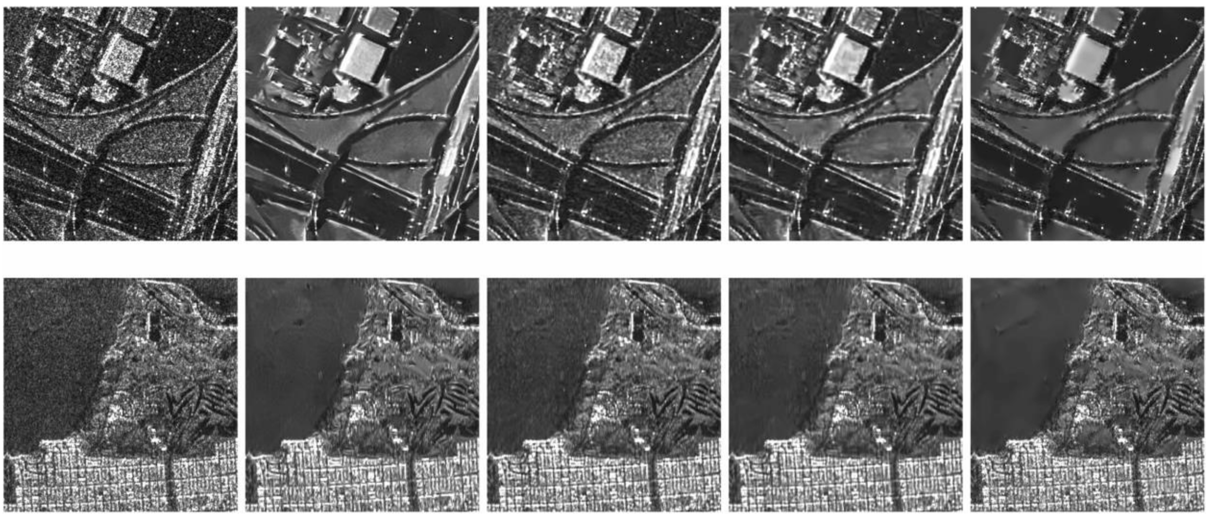

Fig. 5. Results obtained from real SAR images (first row, Toronto (L=1) and second row, San Francisco (L=4)). From left to right, real SAR image, PPB, SARBM3D, FANS, and proposed method despeckling results, respectively.

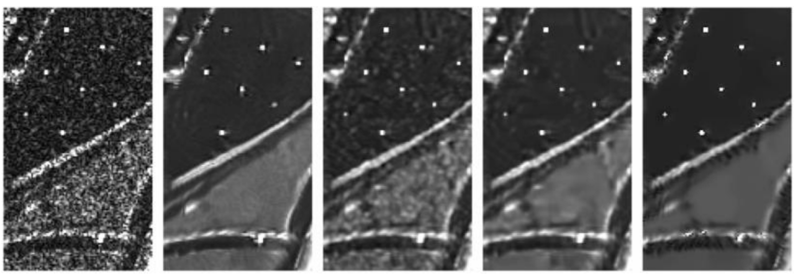

Fig. 6. The zoomed area images. From left to right, real SAR image, PPB, SARBM3D, FANS, and proposed method, respectively.

TABLE II

ENL, EPD-ROA, AND MOR VALUES

Results with Toronto

Despeckling Methods	ENL		EPD-ROA		MoR
	Zone 2	Zone 1	H	V	
PPB	30.933	19.148	0.6693	0.6858	0.863
SAR-BM3D	6.375	5.534	0.6726	0.6893	0.873
FANS	20.166	15.175	0.6640	0.6816	0.856
Proposed	45.894	47.842	0.6775	0.6948	0.995
Results with San Francisco					
Despeckling Methods	ENL		EPD-ROA		MoR
	Zone 2	Zone 1	H	V	
PPB	111.224	73.959	0.9441	0.9368	0.959
SAR-BM3D	24.008	13.514	0.9457	0.9311	0.955
FANS	73.507	27.970	0.9359	0.9171	0.952
Proposed	239.617	291.722	0.9617	0.9473	0.964

IV. Conclusion

This paper proposed a hybrid speckle reduction method for SAR images. The idea in this article was to combine the complex wavelet shrinkage and non-local filtering. Also, to achieve a heterogeneous-adaptive despeckling, a classification stage was added to the algorithm. Experimental results showed that the proposed method provides both effective speckle reduction in homogeneous areas and details preservation altogether. However, due to using UDT-CWT and non-local approach, our proposed method is relatively time-consuming. Furthermore, a few parameters in our method have to be optimally tuned to achieve the best results, which will be the subject of further research works on advanced optimization approaches.

Acknowledgment

The authors would like to thank VILab for providing UDTCWT MATLAB code, as well as Dr. Deledalle for providing the MATLAB code of the PPB filter and GRIP–Image Processing Research Group for providing the SARBM3D and FANS MATLAB codes, as well as benchmarking datasets. The authors would also like to thank the AIRBUS Defense and Space and NASA-JPL for providing the SAR images that are used in this research.

References

[1] J.-S. Lee, “Speckle suppression and analysis for synthetic aperture radar images,” *Opt. Eng.*, vol. 25, no. 5, pp. 636–643, 1986.

[2] V. S. Frost, J. A. Stiles, K. S. Shanmugan, and J. C. Holtzman, “A model for radar images and its application to adaptive digital filtering of multiplicative noise,” *IEEE Trans. Pattern Anal. Mach. Intell.*, vol. PAMI-4, no. 2, pp. 157–166, Mar. 1982.

[3] D. T. Kuan, A. A. Sawchuk, T. C. Strand, and P. Chavel, “Adaptive noise smoothing filter for images with signal-dependent noise,” *IEEE Trans. Pattern Anal. Mach. Intell.*, vol. PAMI-7, no. 2, pp. 165–177, Mar. 1985.

[4] T. Bianchi, F. Argenti, and L. Alparone, “Segmentation-based map despeckling of SAR images in the undecimated wavelet domain,” *IEEE Trans. Geosci. Remote Sens.*, vol. 46, no. 9, pp. 2728–2742, Sep. 2008.

[5] F. Argenti, T. Bianchi, A. Lapini, and L. Alparone, “Fast map despeckling based on Laplacian–Gaussian modeling of wavelet coefficients,” *IEEE Geosci. Remote Sens. Lett.*, vol. 9, no. 1, pp. 13–17, Jan. 2012.

[6] H.-C. Li,W. Hong, Y.-R.Wu, and P.-Z. Fan, “Bayesian wavelet shrinkage with heterogeneity-adaptive threshold for SAR image despeckling based on generalized gamma distribution,” *IEEE Trans. Geosci. Remote Sens*, vol. 51, no. 4, pp. 2388–2402, Apr. 2013.

[7] S. Mallat, “A theory for multiresolution signal decomposition: Thewavelet representation,” *IEEE Trans. Pattern Anal. Mach. Intell.*, vol. 11, no. 7, pp. 674–693, Jul. 1989.

[8] M. I. H. Bhuiyan, M. O. Ahmad, and M. Swamy, “Spatially adaptive wavelet-based method using the cauchy prior for denoising the SAR images,” *IEEE Trans. Circuits Syst. Video Technol.*, vol. 17, no. 4, pp. 500–507, Apr. 2007.

[9] Q. Gao, Y. Lu, D. Sun, Z.-L. Sun, and D. Zhang, “Directionlet-based denoising of SAR images using a Cauchy model,” *Signal Process.*, vol. 93, no. 5, pp. 1056–1063, 2013.

[10] J. J. Ranjani and S. Thiruvengadam, “Dual-tree complex wavelet transform based SAR despeckling using interscale dependence,” *IEEE Trans. Geosci. Remote Sens*, vol. 48, no. 6, pp. 2723–2731, Jun. 2010.

[11] Y. Lu, Q. Gao, D. Sun, and D. Zhang, “Directionlet-based method using the Gaussian mixture prior to SAR image despeckling,” *Int. J. Remote Sens.*, vol. 35, no. 3, pp. 1143–1161, 2014.

[12] D. Hazarika, V. K. Nath, and M. Bhuyan, “SAR image despeckling based on a mixture of Gaussian distributions with local parameters and multiscale edge detection in lapped transform domain,” *Sens. Imag.*, vol. 17, no. 1, p. 15, 2016.

[13] Y. Lu, Q. Gao, D. Sun,Y. Xia, and D. Zhang, “SAR speckle reduction using Laplace mixture model and spatial mutual information in the directionlet domain,” *Neurocomputing*, vol. 173, pp. 633–644, 2016.

[14] D. Hazarika, V. Nath, and M. Bhuyan, “SAR image despeckling based on combination of Laplace mixture distribution with local parameters and multiscale edge detection in lapped transform domain,” *Procedia Comput. Sci.*, vol. 87, pp. 140–147, 2016.

[15] A. Buades, B. Coll, and J.-M. Morel, “A non-local algorithm for image denoising,” in *Proc. IEEE Conf. Comput. Vis. Pattern Recog.*, vol. 2, 2005, pp. 60–65.
[16] C. A. Deledalle, L. Denis, and F. Tupin, “Iterative weighted maximumlikelihood denoising with probabilistic patch-based weights,” *IEEE Trans. Image Process.*, vol. 18, no. 12, pp. 2661–2672, Dec. 2009.
[17] S. Parrilli, M. Poderico, C. V. Angelino, and L. Verdoliva, “A nonlocal SAR image denoising algorithm based on LLMMSE wavelet shrinkage,” *IEEE Trans. Geosci. Remote Sens.*, vol. 50, no. 2, pp. 606–616, Feb. 2012.
[18] D. Cozzolino, S. Parrilli, G. Scarpa, G. Poggi, and L. Verdoliva, “Fast adaptive nonlocal SAR despeckling,” *IEEE Trans. Geosci. Remote Sens. Lett.*, vol. 11, no. 2, pp. 524–528, Feb. 2014.
[19] C. A. Deledalle, L. Denis, F. Tupin, A. Reigber, and M. J¨ager, “A unified nonlocal framework for resolution-preserving (pol)(in) SAR denoising,” *IEEE Trans. Geosci. Remote Sens.*, vol. 53, no. 4, pp. 2021–2038, Apr. 2015.
[20] D. Gragnaniello, G. Poggi, G. Scarpa, and L. Verdoliva, “SAR image despeckling by soft classification,” *IEEE J. Sel. Topics Appl. Earth Observ. Remote Sens.*, vol. 9, no. 6, pp. 2118–2130, Jun. 2016.
[21] G. Di Martino, A. Di Simone, A. Iodice, G. Poggi, D. Riccio, and L. Verdoliva, “Scattering-based SARBM3D,” *IEEE J. Sel. Topics Appl. Earth Observ. Remote Sens.*, vol. 9, no. 6, pp. 2131–2144, Jun. 2016.
[22] X. Ma, H. Shen, X. Zhao, and L. Zhang, “SAR image despeckling by the use of variational methods with adaptive nonlocal functionals,” *IEEE Trans. Geosci. Remote Sens.*, vol. 54, no. 6, pp. 3421–3435, Jun. 2016.
[23] F. Liu, J. Wu, L. Li, L. Jiao, H. Hao, and X. Zhang, “A hybrid method of SAR speckle reduction based on geometric-structural block and adaptive neighborhood,” *IEEE Trans. Geosci. Remote Sens.*, vol. 56, no. 2, pp. 730–748, Feb. 2018.
[24] D. Guan, D. Xiang, X. Tang, and G. Kuang, “SAR image despeckling based on nonlocal low-rank regularization,” *IEEE Trans. Geosci. Remote Sens.*, pp. 1–18, Dec. 2018.
[25] Z. Yu,W.Wang, C. Li,W. Liu, and J. Yang, “Speckle noise suppression in SAR images using a three-step algorithm,” *Sensors*, vol. 18, no. 11, 2018, Art. no. 3643.
[26] X. Ma, P. Wu, Y. Wu, and H. Shen, “A review on recent developments in fully polarimetric SAR image despeckling,” *IEEE J. Sel. Topics Appl. Earth Observ. Remote Sens.*, vol. 11, no. 3, pp. 743–758, Mar. 2018.
[27] X. Ma, P. Wu, and H. Shen, “Multifrequency polarimetric SAR image despeckling by iterative nonlocal means based on a space frequency information joint covariance matrix,” *IEEE J. Sel. Topics Appl. Earth Observ. Remote Sens.*, vol. 12, no. 1, pp. 274–284, Jan. 2019.
[28] G. Chierchia, D. Cozzolino, G. Poggi, and L. Verdoliva, “SAR image despeckling through convolutional neural networks,” in *Proc. IEEE Int. Geosci. Remote Sens. Symp.*, 2017, pp. 5438–5441.
[29] P. Wang, H. Zhang, and V. M. Patel, “SAR image despeckling using a convolutional neural network,” *IEEE Signal Process. Lett.*, vol. 24, no. 12, pp. 1763–1767, Dec. 2017.
[30] X. Tang, L. Zhang, and X. Ding, “SAR image despeckling with a multilayer perceptron neural network,” *Int. J. Digit. Earth*, vol. 12, pp. 1–21, 2018.
[31] D.-Q. Chen and L.-Z. Cheng, “Spatially adapted total variation model to remove multiplicative noise,” *IEEE Trans. Image. Process.*, vol. 21, no. 4, 2012, Art. no. 1650.
[32] D. Gleich, “Optimal-dual-based *l*1 analysis for speckle reduction of SAR data,” *IEEE Trans. Geosci. Remote Sens.*, vol. 56, no. 11, pp. 6674–6685, Nov. 2018.
[33] C. Oliver and S. Quegan, *Understanding Synthetic Aperture Radar Images*. Raleigh, NC, USA: SciTech, 2004.
[34] I. W. Selesnick, R. G. Baraniuk, and N. C. Kingsbury, “The dual-tree complex wavelet transform,” *IEEE Signal Process. Mag.*, vol. 22, no. 6, pp. 123–151, Nov. 2005.
[35] P. R. Hill, N. Anantrasirichai, A. Achim, M. E. Al-Mualla, and D. R. Bull, “Undecimated dual-tree complex wavelet transforms,” *Signal Process. Image Commun.*, vol. 35, pp. 61–70, 2015.
[36] L. Zhang,W. Dong, D. Zhang, and G. Shi, “Two-stage image denoising by principal component analysis with local pixel grouping,” *Pattern Recog.*, vol. 43, no. 4, pp. 1531–1549, 2010.
[37] A. Lopes, E. Nezry, R. Touzi, and H. Laur, “Structure detection and statistical adaptive speckle filtering in sar images,” *Int. J. Remote Sens.*, vol. 13, no. 9, pp. 1735–1758, 1993.
[38] M. K. Mihcak, I. Kozintsev, K. Ramchandran, and P. Moulin, “Lowcomplexity image denoising based on statistical modeling of wavelet coefficients,” *IEEE Signal Process. Lett.*, vol. 6, no. 12, pp. 300–303, Dec. 1999.
[39] M. I. H. Bhuiyan, M. O. Ahmad, and M. Swamy, “Wavelet-based despeckling of medical ultrasound images with the symmetric normal inverse Gaussian prior,” in *Proc. IEEE Int. Conf. Acoust., Speech, Signal Process.*, vol. 1, 2007, pp. 721–724.
[40] D. L. Donoho, “De-noising by soft-thresholding,” *IEEE Trans. Inf. Theory*, vol. 41, no. 3, pp. 613–627, May 1995.
[41] H. Rabbani and S. Gazor, “Image denoising employing local mixture models in sparse domains,” *IET Image Process.*, vol. 4, no. 5, pp. 413–428, Oct. 2010.
[42] H. Xie, L. E. Pierce, and F. T. Ulaby, “Statistical properties of logarithmically transformed speckle,” *IEEE Trans. Geosci. Remote Sens.*, vol. 40, no. 3, pp. 721–727, Mar. 2002.
[43] Y. Cui, G. Zhou, J. Yang, and Y. Yamaguchi, “Unsupervised estimation of the equivalent number of looks in SAR images,” *IEEE Geosci. Remote Sens. Lett.*, vol. 8, no. 4, pp. 710–714, Jul. 2011.
[44] H. Xie, L. E. Pierce, and F. T. Ulaby, “SAR speckle reduction usingwavelet denoising and Markov random field modeling,” *IEEE Trans. Geosci. Remote Sens.*, vol. 40, no. 10, pp. 2196–2212, Oct. 2002.
[45] G. D. Martino, M. Poderico, G. Poggi, D. Riccio, and L. Verdoliva “Benchmarking framework for SAR despeckling,” *IEEE Trans. Geosci. Remote Sens.*, vol. 52, no. 3, pp. 1596–1615, Mar. 2014.

[46] Jan. 29, 2019. [Online]. Available: https://www.charles-deledalle. fr/pages/ppb.php
[47] May 30, 2013. [Online]. Available: http://www.grip.unina.it/research/80-sar-despeckling/80-sar-bm3d.html
[48] Jul. 30, 2013. [Online]. Available: http://www.grip.unina.it/research/86-sar-despeckling/86-fans.html
[49] May 21, 2013. [Online]. Available: http://www.grip.unina.it/research/80-sar-despeckling/85.html
[50] H. Feng, B. Hou, and M. Gong, "SAR image despeckling based on local homogeneous-region segmentation by using pixel-relativity measurement," *IEEE Trans. Geosci. Remote Sens.*, vol. 49, no. 7, pp. 2724–2737, Jul. 2011.